Highly Extended Image States around Nanotubes

Brian E. Granger,[1,*] Petr Král,[1,2,†] H. R. Sadeghpour,[1,‡] and Moshe Shapiro[2,§]

[1]ITAMP, Harvard-Smithsonian Center for Astrophysics, Cambridge, Massachusetts 02138
[2]Department of Chemical Physics, Weizmann Institute of Science, 76100 Rehovot, Israel
(Received 20 June 2002; published 6 September 2002)

We predict that freely suspended, linear molecular conductors or dielectrics, such as carbon nanotubes, can support electronic states that are localized far from the surface. These "tubular image states" are formed in extended potential wells resulting from the tug of war between the external electron's attraction to its image charge in the nanotube, and its repulsion from the tube due to its transverse angular momentum. The displacement of these states (> 10 nm) away from the surface prevents their wave functions from collapsing, resulting in long lifetimes at low temperatures. We predict that tubular image states with binding energies of 1–10 meV can be formed via radiative recombination.

Atomic and molecular Rydberg states are long-lived electronic states, weakly bound to a distant central attractor [1]. Recent advances in the laser and magnetic cooling of atoms and molecules have enabled their exploration in new, unusual settings. For example, large numbers of Rydberg atoms have been reported in an expanding ultracold neutral plasma, where their large electric dipole moments can freeze the atoms into a correlated gas [2]. Long-lived Rydberg molecules have now been detected [3]. Even more exotic Rydberg molecules, with large internuclear separations and dipole moments, have been predicted to exist in ultracold environments [4].

Spatially extended electronic states can also be formed near the surfaces of conductors or dielectrics [5–8]. They occur when an external electron polarizes a surface and becomes attracted to its "image charge" residing below the surface. The resulting interaction potential for an electron at a distance z above a flat surface, with dielectric constant ϵ, is Coulomb-like: $V(z) = -\frac{e^2}{4z}\left(\frac{\epsilon-1}{\epsilon+1}\right)$ [5]. Because of its $1/z$ form, this potential supports an infinite number of "image states" having a familiar Rydberg-series form, $E_n = -\frac{13.60}{16n^2}\left(\frac{\epsilon-1}{\epsilon+1}\right)^2$ eV, where n is the principal quantum number.

As an example, Höfer *et al.* [9] have used two-photon photoemission to populate coherent wave packets of image states above a Cu(100) surface. The observed states had $n \sim 7$, binding energies of 15–40 meV, and lifetimes of a few picoseconds, which were limited by the rapid collapse of the states into the Cu(100) surface. Image states with higher n have longer lifetimes $\tau_n \sim n^3$ [10], but weaker binding energies, since the latter scale as $1/n^2$. Similar experiments performed above molecular wires laid on surfaces [11], nanoparticles [12,13], and one- and two-dimensional liquid He [14] demonstrate that extended image states are common in nanoscopic systems.

In this work, we predict the existence of a class of spatially extended "tubular image states" that form around the surfaces of freely suspended linear molecular conductors or dielectrics, and, in particular, around *metallic nanotubes* (see Fig. 1) [15,16]. While the physical principles governing the existence of these states are analogous to the usual image states, these tubular image states can be prepared with *nonzero angular momentum*, l. The resulting centrifugal barrier keeps the electronic wave functions away from the surface of the tube, thereby reducing the rate of collapse of the image states into the surface and increasing their lifetimes.

To describe a tubular image state (TIS), we begin by deriving the interaction potential $V(\rho_0)$ between a nanotube of radius a and an electron at a distance ρ_0 from its axis. At the large distances relevant here ($\rho_0/a \gg 1$), nanotubes can simply be characterized by a frequency dependent dielectric tensor $\underline{\epsilon}(\omega)$ [17]. *Ab initio* calculations
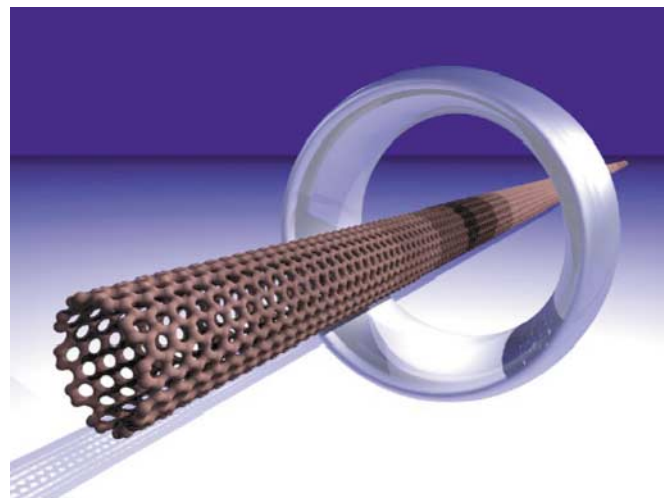

FIG. 1 (color online). A visualization is shown of an electron in a tubular image state (TIS) around a (10, 10) metallic carbon nanotube. States having large radii (> 10 nm) are formed in the interaction potential of Eq. (6). Similar states should exist around any metallic or semiconducting nanotube, including multiwalled or ring-shaped nanotubes.

show [18] that metallic nanotubes can be described, in first approximation, as perfectly conducting, infinitely long, cylinders (for which $\underline{\varepsilon} \approx \infty$); the modifications required to treat dielectric nanotubes will be sketched below. In either case, the image potential for the cylindrical geometry is significantly more complicated than that of the planar and spherical configurations.

When a charge q approaches a metallic nanotube, it polarizes the tube, inducing a scalar potential Φ_{ind}. The total scalar potential $\Phi_{tot} = \Phi_0 + \Phi_{ind}$ is the sum of the potential due to the external charge Φ_0, and the induced potential Φ_{ind}. By requiring that Φ_{tot} vanishes on the tube's surface, the induced potential is found to be [19],

$$\Phi_{ind}(\rho, \varphi, z) = -\frac{2q}{\pi} \sum_{m=-\infty}^{m=+\infty} \int_0^\infty dk \cos(kz) \exp(im\phi)$$
$$\times \frac{I_m(ka)}{K_m(ka)} K_m(k\rho_0) K_m(k\rho), \quad (1)$$

where the electron is located outside the tube at the position $(\rho_0, 0, 0)$, and $(I_m(x), K_m(x))$ are the regular and irregular modified Bessel functions.

The interaction potential (energy) is defined as

$$V(\rho_0) = \frac{1}{2} q \, \Phi_{ind}(\rho_0, 0, 0), \quad (2)$$

where the factor of $1/2$ eliminates double counting of the energy [20]. The potential's long-range behavior emerges most transparently when the electrostatic force between the charge and the conducting cylinder is calculated by differentiating Eq. (1) with respect to ρ:

$$F(\rho_0) = -q \partial \Phi_{ind}/\partial \rho |_{(\rho_0,0,0)}$$
$$= \frac{2q^2}{\pi a^2} \int_0^\infty dx \left[A_0(x) + 2 \sum_{m=1}^\infty A_m(x) \right], \quad (3)$$
$$A_m(x) = \frac{I_m(x)}{K_m(x)} K_m(x\rho_0/a) x K'_m(x\rho_0/a).$$

Asymptotic analysis shows that, at large distances $(\rho_0/a \gg 1)$, the induced force $F(\rho_0)$, Eq. (3), is dominated by the $m = 0$ term. Then, the long-range potential $V(\rho_0) = -\int^{\rho_0} F(\rho) d\rho$ calculated from Eq. (3) with the $m = 0$ term takes on the simple form

$$V(\rho_0) \sim \frac{q^2}{a} \mathrm{li}\left(\frac{a}{\rho_0}\right) \approx -\frac{q^2}{a} \frac{1}{(\rho_0/a) \ln(\rho_0/a)}, \quad (4)$$

where $\mathrm{li}(x) \equiv \int_0^x dt/\ln(t)$ is the logarithmic integral [21].

Equation (4) agrees with the expectation, based on geometrical grounds [20], that at large distances the result for the conducting cylinder should lie somewhere between that of a conducting plane $(V \sim -1/z)$ and a conducting sphere $(V \sim -1/r^2$, where r is the radial distance).

Motivated by the long-range form of the potential, Eq. (4), we construct the following approximate potential,

$$V(\rho_0) \approx \frac{2}{\pi} \frac{q^2}{a} \sum_{n=1,3,5,\dots} \mathrm{li}[(a/\rho_0)^n], \quad (5)$$

by modifying, *ad hoc*, the long-range force $F(\rho_0)$ to have the correct behavior near the surface of the nanotube, where $F(\rho_0) \sim 1/|\rho_0 - a|^2$. Thus, while only approximate, Eq. (5) has the correct limiting behavior close to the nanotube $(\rho_0/a \sim 1)$ as well as far from it [22]. Moreover, it reproduces the exact result [obtained by numerically integrating Eqs. (1) and (2)] to within a few percent for the values of (ρ_0/a) relevant in this work.

The above results, valid for a metallic cylinder $(\underline{\varepsilon} \approx \infty)$, can be extended to a cylinder with a finite anisotropic dielectric tensor ε_{ij}. If we assume a uniform tube, the tensor can be diagonalized to yield three components: one along the tube axis (ε_{zz}) and two $(\varepsilon_{xx}, \varepsilon_{yy})$ perpendicular to it. Because of the nonconductance of single or multi-walled nanotubes in the transverse direction, $\varepsilon_{xx} = \varepsilon_{yy}$ is typically small even when ε_{zz} is large. Including a finite anisotropic dielectric function in the above derivation shows that the leading correction to the interaction potential $V(\rho_0)$ of Eqs. (1) and (2) scales as $1/\sqrt{\varepsilon_{zz}\varepsilon_{xx}}$. Thus, as long as the dielectric function is large along the tube, that is $\varepsilon_{zz}\varepsilon_{xx} \gg 1$, the interaction potential is practically identical to the perfectly conducting case.

The effective interaction potential $V_{eff}(\rho)$ is formed by combining the attractive induced potential, Eq. (5), and the repulsive centrifugal potential:

$$V_{eff}(\rho) = V(\rho) + \frac{(l^2 - \frac{1}{4})}{2\mu\rho^2}, \quad (6)$$

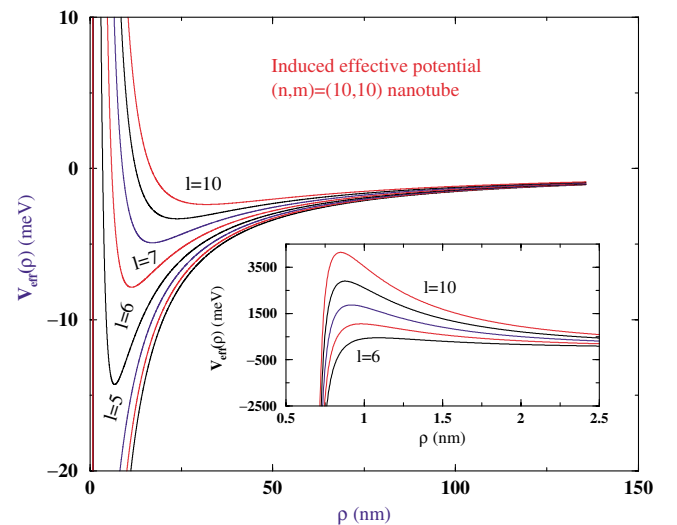where μ is the reduced mass of the charged particle. Figure 2 shows the effective potential $V_{eff}(\rho)$ for an

FIG. 2 (color online). The effective potential $V_{eff}(\rho)$ between an electron and a conducting nanotube is shown for a number of angular momenta l. Extremely long-range minima are seen, which support a series of bound TISs. The inset shows a blowup of the potentials near the nanotube ($\rho \approx 0.5$–2.5 nm), where large (1–2 eV) potential barriers exist.

electron ($\mu = m_e = q = 1$ in atomic units) in front of a (10,10) metallic carbon nanotube of radius $a = 0.68$ nm. For moderate angular momenta ($l \gtrsim 6$), the effective potential possesses extremely long-range wells that support bound TISs. The inset of Fig. 2 shows that high (1–2 eV) potential barriers separate these wells from the tube surface.

The electronic motion in the vicinity of a nanotube can be localized in the longitudinal z direction by external electrodes, structures, or defects (with different dielectric properties) that are formed inside the tube or on its surface. Such inhomogeneities can also localize electrons inside quantum dots having lengths of a few hundred nanometers, a phenomenon observed recently in carbon nanotubes [23].

The total electronic wave function is written in a separable form as $\Psi_{n,l,k}(\rho, \varphi, z) = \psi_{n,l}(\rho)\, e^{i l \varphi} \phi_k(z)/\sqrt{2\pi\rho}$, so that the motion along the tube ($\hat{z}$) separates out and the total energy becomes $E_{n,l,k} = E_{n,l} + E_k$. In this paper we focus primarily on the transverse energy $E_{n,l}$ and wave function $\psi_{n,l}(\rho)$, which satisfy the Schrödinger equation

$$\left(\frac{d^2}{d\rho^2} + 2\mu[E_{n,l} - V_{\text{eff}}(\rho)]\right)\psi_{nl}(\rho) = 0. \qquad (7)$$

The longitudinal energy E_k is either continuous ($E_k = k^2/2$) or quantized depending on whether the electron is localized in the $\hat{z}$ direction or not.

Figure 3 shows the $n = 1$ transverse wave functions $\psi_{n=1,l}(\rho)$ for the potentials of Fig. 2. They show that, even for moderate angular momenta l, the electron is kept a substantial distance (10–50 nm) away from the nanotube's surface, with ρ_{max}, the distance of maximum

probability, scaling as $\rho_{\text{max}} \sim l^3$. The associated binding energies $E_{n,l}$ are presented in Fig. 4. The long-range form of the interaction potential, Eq. (4), gives rise to an n- and l-dependent series of energy levels (1–10 meV), which scale as $E_{n,l} \sim l^{-3}$ for fixed n.

We now briefly discuss the decay mechanisms of the TISs. For general image states, the most important decay channel is the collapse of the external electron into the bulk, which is controlled by the overlap of the image wave functions with the surface states [7,9]. For TISs with moderate angular momenta this decay is suppressed by the centrifugal barrier. For a barrier of height $h \sim$ 1–2 eV and width $w \approx 0.5$–2 nm (see inset in Fig. 2), the tunneling lifetimes can be estimated as $\tau \approx 2w/v\,|T|^2$, where $|T|^2$ designates the transmission coefficient, $|T|^2 = \exp[-\int d\rho\,[2\mu\,[V(\rho) - E_{n,l}])^{1/2}] \sim \exp(-\sqrt{h}w)$, and v is the electron velocity. The typical binding energies in Fig. 4 of 10 meV lead to $|T|^2 \sim 10^{-9}$ and lifetimes of $\tau \sim 0.1$ ms. These lifetimes increase exponentially with l and are substantially longer than those of image states above planar surfaces.

In contrast to atomic and molecular Rydberg states, electrons in TISs interact dynamically with holes in the nanotube when the image potential is induced. Therefore, scattering of the holes can dramatically reduce the TIS lifetimes, because any fluctuation in the potential $V_{\text{eff}}(\rho)$ can induce transitions between the image states and even ionize them. In addition, the coupling of TISs to phonons in the tube will produce similar effects. These decay mechanisms can be suppressed by working at temperatures ($T < 10$ K) lower than the transition energy between different tubular image states.
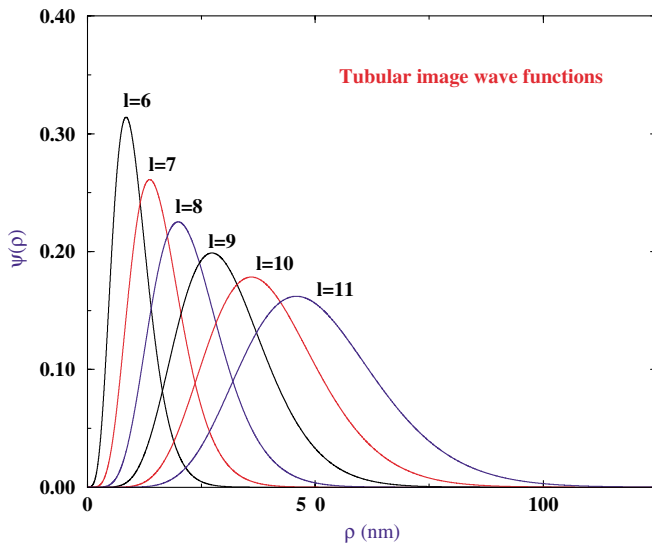

FIG. 3 (color online). The $n = 1$ wave functions $\psi_{n=1,l}(\rho)$ are shown for the effective potentials $V_{\text{eff}}(\rho)$ of Fig. 2. The wave functions have maxima, whose distances from the tube surface scale as $\rho_{\text{max}} \sim l^3$.
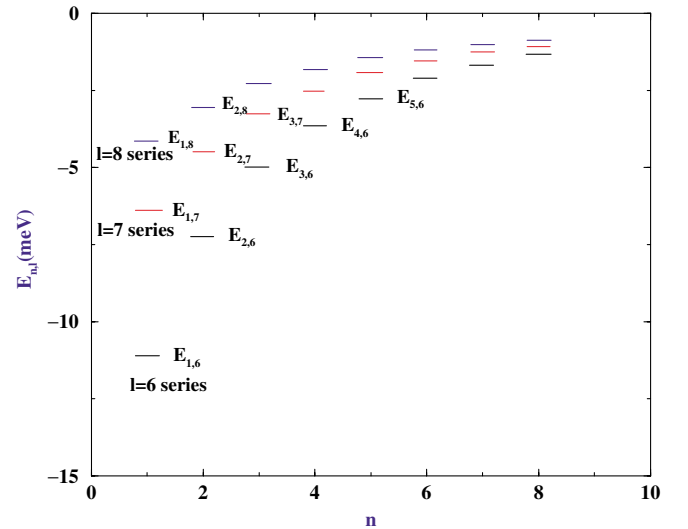

FIG. 4 (color online). Tubular image states have binding energies $E_{n,l}$ in the 1–10 meV range. Unlike Coulombic image potentials, eigenenergies having the same principal quantum number n, but different angular momentum l are nondegenerate. The $n = 1$ states shown correspond to the wave functions in Fig. 3.

Spontaneous radiative transitions between different tubular image states also limit their lifetimes. These depend on the transition oscillator strength from an initial state $|n_i l_i\rangle$ to a final state $|n_f l_f\rangle$: $f_{n_f n_i} = (E_f - E_i)|\langle n_f l_f|\rho e^{i\phi}|n_i l_i\rangle|^2$, where $l_f = l_i \pm 1$ for the emission of circularly polarized light. Using the wave functions of Fig. 3, we have calculated the radiative lifetimes for several tubular image states and found them to be 5–10 ms [22]. Stimulated transitions due to blackbody radiation will shorten these lifetimes somewhat [1].

Tubular image states can be formed by inverse photoemission (radiative recombination), which has already been used to populate low-energy image states in front of Cu, Ag, Sb, and Au surfaces [8]. The cross section for radiative recombination behaves as $\sigma^{rr} \sim E^{-1}$ at low electron energies, and is related to the cross section for photoionization by the detailed balance condition, $\sigma_{nl}^{rr}(\omega) = (\frac{\omega}{ck})^2 \sigma_{nl}^{pi}(\omega)$ [24], where ω is the photon energy and $E = \frac{k^2}{2}$ is the electron kinetic energy. We have calculated the photoionization cross section using the bound wave functions of Fig. 3 and energy-normalized WKB wave functions [25] to represent the continuum states. At electron energies of $E \sim 10$ meV, (generated, for example, by emission from the tips of other nanotubes [26]), we find the recombination cross sections to be $\sigma^{rr} \sim 10^{-18} - 10^{-17}$ cm^2, corresponding to rate coefficients of $\alpha^{rr} \sim 10^{-13} - 10^{-12}$ cm^3 s^{-1}. For electron-beam densities of $n_e \sim 10^{15}$ cm^{-3}, each nanotube will acquire an extra electron in a TIS within 0.1–1 ms.

Tubular image states may prove to be a universal feature of nanoscopic cylindrical conductors and dielectrics. They provide a new setting in which to investigate extended (Rydberg-like) states. Their long lifetimes and moderate binding energies should make possible the study of a number of phenomena. First, the long-range interactions could be probed by electron interferometry, a method that has already been used to probe the van der Waals forces in atoms [27]. Such image states could be used as nanoscopic charged particle storage rings. Finally, because the details of the tubular image states depend directly on the nanotube properties, such as $\underline{\epsilon}(\omega)$, spectroscopy of such states should also provide valuable information about the nanotube itself.

*Email address: bgranger@cfa.harvard.edu
†Email address: kral@weizmann.ac.il
‡Email address: hsadeghpour@cfa.harvard.edu
§Email address: moshe.shapiro@weizmann.ac.il

[1] T. Gallagher, *Rydberg Atoms* (Cambridge University Press, New York, 1994).
[2] T. C. Killian *et al.*, Phys. Rev. Lett. **86**, 3759 (2001); W. R. Anderson, J. R. Veale, and T. F. Gallagher, *ibid.* **80**, 249 (1998).
[3] W. G. Scherzer *et al.*, Phys. Rev. Lett. **72**, 1435 (1994).
[4] C. H. Greene, A. S. Dickinson, and H. R. Sadeghpour, Phys. Rev. Lett. **85**, 2458 (2000); B. E. Granger, E. L. Hamilton, and C. H. Greene, Phys. Rev. A **64**, 042508 (2001).
[5] N. D. Lang and W. Kohn, Phys. Rev. B **7**, 3541 (1973); R. Shakeshaft and L. Spruch, Phys. Rev. A **31**, 1535 (1985).
[6] P. M. Echenique, F. Flores, and F. Sols, Phys. Rev. Lett. **55**, 2348 (1985); E. V. Chulkov *et al.*, *ibid.* **80**, 4947 (1998); S. Schuppler *et al.*, Phys. Rev. B **46**, 13 539 (1992); J. Osma *et al.*, Phys. Rev. B **59**, 10 591 (1999).
[7] M. Wolf, E. Knoesel, and T. Hertel, Phys. Rev. B **54**, R5295 (1996).
[8] D. Straub and F. J. Himpsel, Phys. Rev. B **33**, 2256 (1986).
[9] U. Höfer *et al.*, Science **277**, 1480 (1997).
[10] P. M. Echenique and J. B. Pendry, Prog. Surf. Sci. **32**, 111 (1990).
[11] J. E. Ortega *et al.*, Phys. Rev. B **49**, 13 859 (1994); I. G. Hill and A. B. McLean, Phys. Rev. Lett. **82**, 2155 (1999).
[12] V. Kasperovich *et al.*, Phys. Rev. Lett. **85**, 2729 (2000).
[13] M. Boyle *et al.* Phys. Rev. Lett. **87**, 273401 (2001).
[14] P. M. Platzman and M. I. Dykman, Science **284**, 1967 (1999); P. Glasson *et al.*, Phys. Rev. Lett. **87**, 176802 (2001).
[15] S. Iijima, Nature (London) **354**, 56 (1991); J. W. Mintmire, B. I. Dunlap, and C. T. White, Phys. Rev. Lett. **68**, 631 (1992); *Carbon Nanotubes: Synthesis, Structure, Properties and Applications*, edited by M. S. Dresselhaus, G. Dresselhaus, and Ph. Avournis (Springer-Verlag, Berlin, 2000).
[16] T. W. Odom, J. L. Huang, P. Kim, and C. M. Lieber, Nature (London) **391**, 62 (1998); J. W. G. Wildöer, *ibid.* **391**, 59 (1998).
[17] L. X. Benedict, S. G. Louie, and M. L. Cohen, Phys. Rev. B **52**, 8541 (1995).
[18] L. Lou, P. Nordlander, and R. E. Smalley, Phys. Rev. B **52**, 1429 (1995).
[19] N. R. Arista and M. A. Fuentes, Phys. Rev. B **63**, 165401 (2001).
[20] J. D. Jackson, *Classical Electrodynamics* (John Wiley & Sons, New York, 1975), 2nd ed.
[21] *Handbook of Mathematical Functions*, edited by M. Abramovitz and I. A. Stegun (Dover Publications, Inc., New York, 1970).
[22] B. E. Granger, H. R. Sadeghpour, and P. Král (to be published).
[23] M. T. Woodside and P. L. McEuen, Science **296**, 1098 (2002).
[24] I. I. Sobelman, *Atomic Spectra and Radiative Transitions*, Chemical Physics 1 (Springer-Verlag, Berlin, 1977).
[25] M. Aymar, C. H. Greene, and E. Luc-Konig, Rev. Mod. Phys. **68**, 1015 (1996).
[26] A. G. Rinzler *et al.*, Science **269**, 1550 (1995).
[27] H. Batelaan (private communication).